Relationship between single and bulk mechanical properties for zeolite ZSM5 spray-dried particles

Relationship between single and bulk mechanical properties for zeolite ZSM5 spray dried particles

M. Marigo[*,a,b], D . L. Cairns[a], J. Bowen[b], A. Ingram[b] and E. H. Stitt[a]

[a] Johnson Matthey Technology Centre, P.O. Box 1, Belasis Avenue, Billingham, Cleveland, TS23 1LB, United Kingdom

[b] Centre for Formulation Engineering, Chemical Engineering, School of Engineering, The University of Birmingham, B15 2TT, United Kingdom

Abstract

In this work the typical mechanical properties for the catalyst support material, ZSM5 zeolite particles, have been measured in order to relate the bulk behaviour of the powder material to the single particles mechanical properties. Particle shape and size distribution of the powders were determined by laser diffraction and Scanning Electron Microscopy (SEM) confirmed the spherical shape of the spray dried particles. The excellent flowability of the material was assessed by typical methods such as the Hausner ratio and the Carr's index. This was confirmed by bulk measurements of particle-particle internal friction parameter and flow function using a Schulze shear cell, which also illustrated the poor compressibility of the material. A single particle compression technique was used for characterising individual particle mechanical properties such as reduced elastic modulus and strength by applying the Hertz contact mechanic theory. Furthermore, nanoindentation was employed to measure particle surface mechanical properties such as hardness and elastic modulus. The latter two methods gave different mechanical properties in terms of reduced elastic modulus showing the mechanical non-homogeneity between the surface of the particle and the entire particle. Finally, particle bulk compression was used to show the influence of single particle mechanical properties on bulk compression behaviour and the Adams model was shown to be suitable for describing the bulk compression. The predicted Adams model parameter, apparent strength for the single particles was in good agreement with the single particle strength determined by single particle compression test. This work illustrates the importance of a comprehensive understanding of particles properties in order to predict or understand the bulk behaviour of powder material during a specific process such as powder compaction.

Keywords: zeolite particle; flowability Powder flow function; Effective angle of internal friction; Schulze shear cell; Nanoindentation; Single particle compression; Bulk compression

1. Introduction to bulk powder compaction: Adams model

Bulk powder compression consists of compacting materials in a die to produce a coherent structure, namely tablets. Compression behaviour of the powder is an important characteristic since it influences the final tablet properties. The powder compaction process depends on a number of different factors and particle properties such as: powder flowability and particle size distribution, shape, hardness, strength, and friction. However, the relation between single particle properties and bulk compression behaviour is not yet well understood (Samimi, Hassanpour, & Ghadiri, 2005). Powder compression studies are widely reported in literature for compression of powders with very different physical properties such as metal powder (Gan, & Gu 2008; Sivasankaran, Sivaprasad, Narayanasamy, & Iyer, 2010), pharmaceutical (Michrafy, Ringenbacher, & Tchoreloff, 2002; Zhang, Seville, Adams, & Yap 2006; Yap, Adams, Seville, & Zhang 2008; Frenning, Nordström, & Alderborn 2009; Klevan, Nordström, Bauer-Brandl, & Alderborn 2009; Klevan, Nordström, Tho, & Alderborn 2010) and ceramic materials (Caligaris, Topolevsky, Maggi, & Brog, 1985, Djuri, Marinkovi-Neduin, Ranogajec, & Radeka, 1995; Ramakrishnan, Nagarajan, RamaRao, & Venkadesan, 1997; Vogler, Lee, & Grady, 2007). In Figure 1 a general schematic of the micromechanics and deformation mechanisms that occurs during bulk compression are illustrated (Stasiak, Tomas, Molenda, Rusinek, & Mueller, 2010).

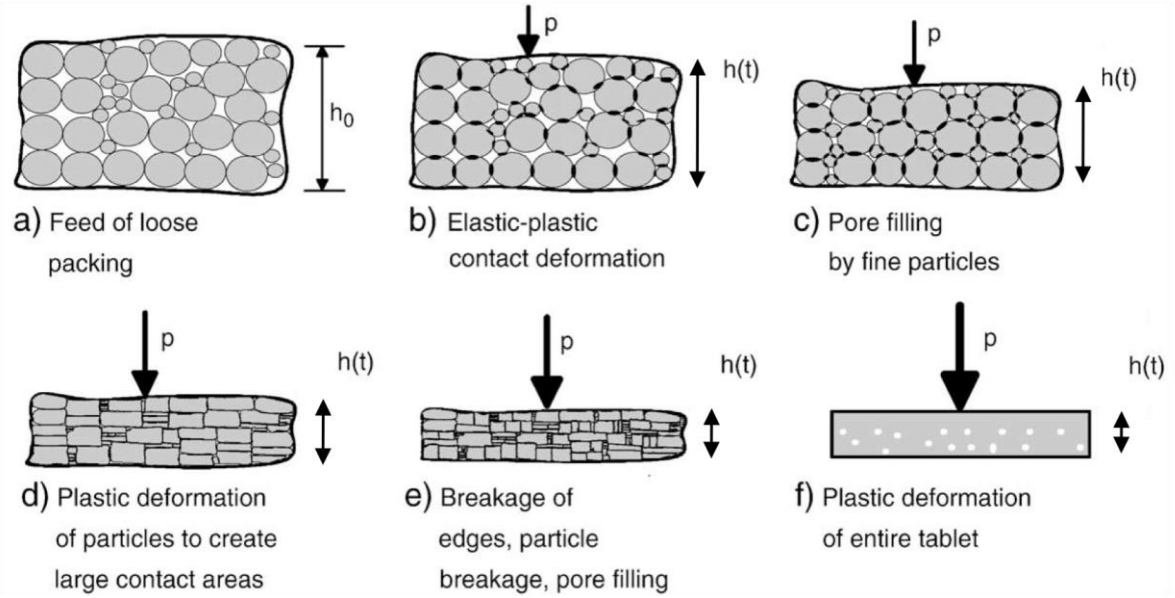

Figure 1: Typical sequences of mechanisms during powder compression.

h_o is the initial bed height and *h(t)* is the value at the current applied pressure *P*. Initially, during compression, loosely packed particles translate and rotate at relatively small contact deformations. Subsequently, particles deform and break as a result of the increase in the elastic-plastic contact stresses. Finally, the entire tablet plastically deforms. The influence and the extent of the described steps depend on the physical and mechanical properties of the particulate material that is undergoing compression.

The Adams et *al.* (1994) model can be employed to correlate volume reduction with pressure applied during compression. The Adams model is a theoretical model for the confined uniaxial compression of agglomerates based on a first-order lumped-parameter analysis for the compression process. The failure of single particles within a column of particles is due to the uniaxial compression stress *P*, constrained by the radial stress P_l that acts laterally on the neighbouring particles. The relationship between the bed pressure *P* and the bed height *h* is:

$$dP = -k_2 \tau \frac{dh}{h} \qquad (1)$$

where k_2 is a constant. The Adams model was developed to estimate the fracture strength of single granules from the Mohr-Coulomb failure criterion, which was employed to explain the macroscopic failure stress. In this criteria, the shear failure stress, τ is related to the sum of the cohesive strength, τ_o and the frictional stress, αP_l, acting at the failure plane as follows:

$$\tau = \tau_o + \alpha P_l \tag{2}$$

α is defined as the lateral pressure coefficient. It was also assumed that the force *F*, the failure force of the weakest granule in the axial direction, is proportional to the product of the failure stress τ and the cross-sectional area of the fracture plane, *A*, as follows

$$F = k_1 \tau A \tag{3}$$

where k_1 is a proportional constant. By including Eq.(2) into Eq.(1) and considering that lateral pressure P_l is related to the axial pressure by the constant k_3, ($P_l = k_3 P$) the following equation is derived:

$$\ln P = \ln\left(\frac{\tau_o^{'}}{\alpha^{'}}\right) + \alpha^{'} \varepsilon_n + \ln\left(1 - e^{\left(-\alpha^{'}\varepsilon_n\right)}\right) \tag{4}$$

where $\tau_o^{'}$ is the apparent strength of the single particles and $\alpha^{'}$ is the apparent coefficient of friction and $\varepsilon_n = \ln\left(h_o / h\right)$ is the natural bed strain. At high stress the last term of Eq.(4) becomes negligible and can be eliminated, leaving a linear function. The slope and intercept of the linear part of the graph can be used to calculate the Adams parameters $\tau_o^{'}$ and $\alpha^{'}$. The previous parameters are related to τ_o and α:

$$\tau_o^{'} = k_2 \tau_o \tag{5}$$

$$\alpha^{'} = k_2 k_3 \alpha \tag{6}$$

2. Material and methods

2.1 ZSM5 zeolite spray dried particles

A spray dried ZSM5 zeolite has been chosen in this work. Zeolite material is widely used in the catalyst industry. The zeolite particles have a skeletal material density (this is determined by considering the volume within the particle envelope minus volume of open pores) of about 2.41 g cm^{-3}, according to helium pycnometry and an average interparticle pore size of 40 Å, as measured by mercury porosimetry.

2.2 Particle shape and size: scanning electron microscopy (SEM) and laser diffraction

In this work, the spray dried zeolite particle size distribution has been determined by laser scattering technique. Particle morphology has been characterized by scanning electron microscopy (SEM). Grain shape is one of the key factors affecting the flow properties of granular material. The technique can provide information regarding: size, shape and surface morphology, which are critical parameters for powder processing and development. Laser light diffraction is an indirect measurement technique where the particle size distribution is inferred from light-scattering measurements. The *Malvern Mastersizer 2000* laser light diffraction was used to gather information about the particle size distribution.

2.3 Single particle characterisations: strength, reduced Young's modulus and hardness

2.3.1 Micromanipulation: single particle compression

Single particle compression can give measurements of mechanical properties such as elastic modulus *E*. The breakage behaviour of the zeolite particles was investigated by the compression of a single particle. The elastic contact for spherical regular particle compressed between two flat rigid surfaces can be described by Hertz et *al.* (1882) theory. During compression of a single particle with a flat punch the contact area deforms and the force *F* versus the displacement *s* can be measured, Figure 2.a.

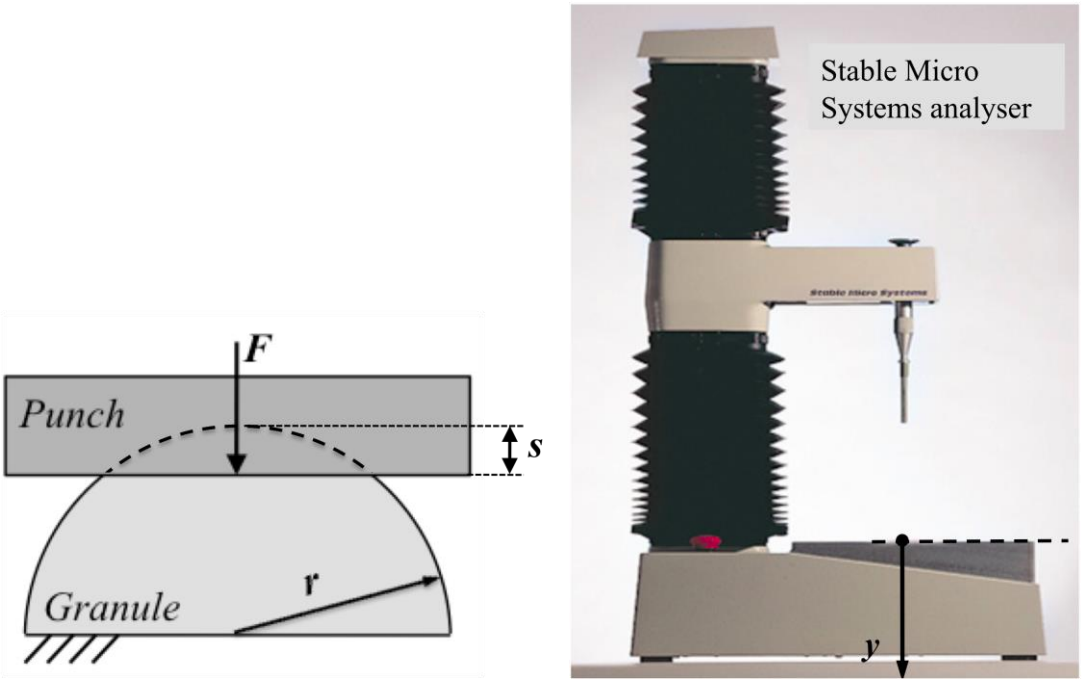

Figure 2: (a) Characteristic plate–particle contact during single particle compression. (b) Stable Microsystems analyser (Stable Micro System LTD, 2010.).

The Stable Micro Systems analyser mechanical testing machine, shown in Figure 2.b by using a stainless steel cylindrical tip probe of 2 mm diameter.

The relationship between the force, *F*, and the relative local displacement of the plates at each contact point, *s*, is as follows:

$$F = \frac{4}{3} r^{1/2} E^* s^{3/2} \qquad (7)$$

where r and E^* are the radius and equivalent (or reduced) Young's modulus of the particle. s is the probe height. The effective modulus of elasticity E^* of both particle (index 1) and punch, made in stainless steel, (index 2) is given (usually $E_2 >> E_1$) as:

$$E^* = \left(\frac{1-\nu_1^2}{E_1} + \frac{1-\nu_2^2}{E_2} \right)^{-1} \approx \left(\frac{1-\nu_1^2}{E_1} \right)^{-1} \quad (8)$$

The peak critical compression force F_{cr} recorded just before particle failure can be used to calculate the particle crushing strength σ_{cr}, Eq.(9) , (Samimi et *al.*, 2005).

$$\sigma_{cr} = \frac{F_{cr}}{\pi r^2} \quad (9)$$

2.3.2 Nanoindentation

Nanoindentation is a measurement technique that allows the determination of mechanical properties such as hardness H or reduced elastic Young's modulus E^*. This technique has been widely used to characterize mechanical properties of powders, especially in the case of pharmaceutical materials (Lin, Shu, & Dong , 2005).

It consists of the loading and unloading of an indent tip against the surface of the material. A typical loading-unloading hysteresis curve is shown in Figure 3 and the three parameters obtained during the measurement are P_{max}, the load measured at a maximum depth of penetration h and A the projected area of contact between the indenter and sample at P_{max}.

The material properties hardness H and the combined modulus of the system, or reduced indentation modulus E^* can be obtained from indentation load-displacement data. Nanoindentation tests were performed using an MML NanoTest™ nanoindenter (MicroMaterials) with a diamond three-sided pyramid-shaped Berkovich-type indenter tip with a half-angle of 65.3° from vertical axis (Wimmer, Lucas, Tsui, & Oliver, 1997).

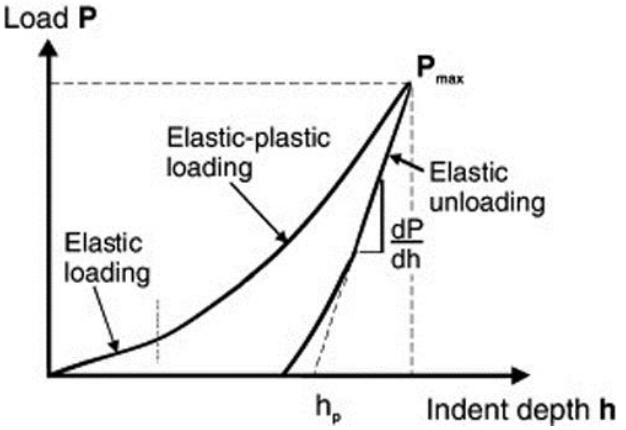

Figure 3: Schematic of a typical load–displacement curve during an indentation test (Meier et *al.*, 2009).

The combined modulus of the system, or reduced indentation modulus E^* is determined from the following expression (Meier, John, Wieckhusen, Wirth, & Peukert, 2009):

$$E^* = \frac{1}{2}\sqrt{\frac{\pi}{A}}\frac{1}{\beta}\frac{dP}{dh} \quad (10)$$

where $\frac{dP}{dh}$ is the gradient of the tangent on the initial unloading curve on the load–displacement plot, Figure 3, β is a geometric correction factor equals to 1.034 for a Berkovich indenter and A is the nominal contact area.

The reduced indentation modulus takes into account the compliance of the diamond indenter tip ($E_i >> E$) as follows:

$$E^* = \left(\frac{1-\nu^2}{E} + \frac{1-\nu_i^2}{E_i} \right)^{-1} \approx \left(\frac{1-\nu^2}{E} \right)^{-1} \quad (11)$$

where E and ν are Young's modulus and Poisson's ratio for the specimen and E_i and ν_i are modulus and Poisson's ratio for the indenter. The hardness can be calculated as:

$$H = \frac{P_{\max}}{A} \quad (12)$$

2.4 Powder flowability

2.4.1 Poured and tapped density: Carr's index and Hausner ratio

The flowability of a powder is a important variable during bulk compression as it has an important effect during the die filling but interparticle friction has an effect during the initial stage of compression when particles rearrange. Flowability of a bulk of powder material depends on many factors, such as particle size, particle shape, size distribution, packing, density, surface properties but also processing conditions like moisture contents, temperature, humidity, electric charge and the applied shear/stress.

In this work the flowability for the ZSM5 zeolite, has been assessed using a indirect method by evaluation of packing properties (Hausner's ratio HR, Carr's compressibility index CI) and by a direct method by determination of the flow function *ffc* using Schulze ring tester.

The Hausner Ratio and Carr Index are two parameters based on the measurement of the poured packing density and the tapped density and their classifications for assessing the flowability are presented in Table 1. The Hausner Ratio is given in Eq.(13), where ρ_{tapped} is the powder bulk density, and ρ_{bulk} is the powder tapped density.

$$HR = \frac{\rho_{tapped}}{\rho_{bulk}} \quad (13)$$

The *bulk density* or *poured density* of the powder (random loose packing) is defined as the ratio between the sample mass and its total volume, which includes the interstices between particles. The *tapped density* (random dense packing) is the value of the bulk density after tapping the container a number of times.

The Carr's Index or compressibility index is calculated as given in Eq.(14).

$$CI = \frac{\left(\rho_{tapped} - \rho_{bulk}\right)}{\rho_{bulk}} \cdot 100\% \quad (14)$$

Table 1: Classification of flowability by Hausner Ratio HR (Hausner, 1967) and Carr's index (Greyand et al., 1969).

Flowability	**HR**
Non flowing	>1.4
Cohesive	>1.4
Fairly free-flowing	1.25-1.4
Free-flowing	1-1.25
Excellent flowing	1-1.25
Aerated	1-1.25

Flowability	**CI %**
Very, very poor	>38
Very poor	32-37
Poor	26-31
Passable	21-25
Fair	16-20
Good	11-15
Excellent	<10

To determine the initial bulk density the sample was poured into a glass cylinder and the volume and mass of the untapped bulk was determined. The sample was then subjected to a numbers of taps (N=1500 times) by using *Copley tap density volumeter model JV200* apparatus.

2.4.2 Schulze shear cell flow function: flow function (ffc)

A consolidated bulk material will start to flow, incipient flow, when sufficient stress is applied. The limit at which the bulk material fails and starts to flow is represented by the *yield locus* represented in Figure 4. Each point on the yield locus is determined as relationship between the measured shear force as a function of the applied normal loads (Schulze, 2006).

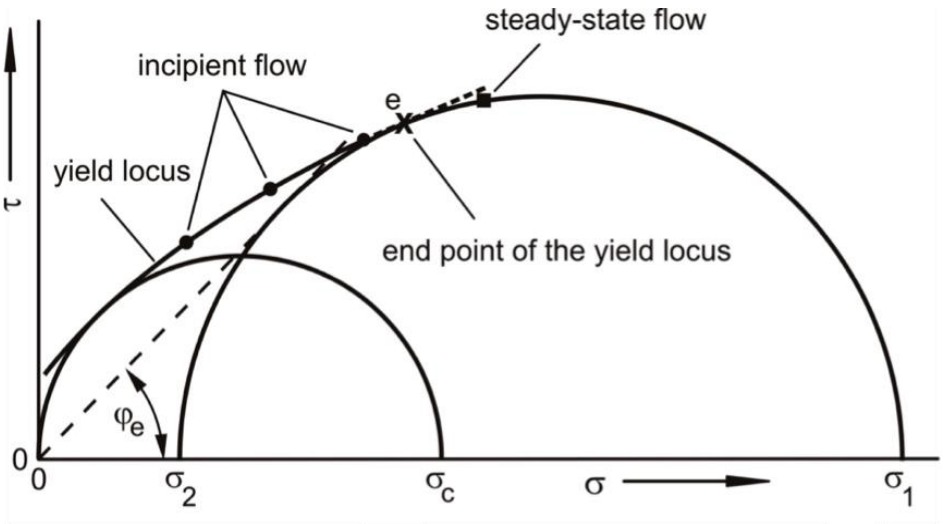

Figure 4: Yield locus and Morh's circles (Schulze, 2006).

The yield locus and corresponding Mohr's circles can be used to predict how easily a particulate material would flow under those conditions by defining the flow function (*ffc*), Eq.(15) (Jenike, 1964). σ_1 and σ_c are defined as consolidation stress and unconfined yield strength. The classification for the flowability based on the *ffc* is reported in Table 2.

$$ff_c = \frac{\sigma_1}{\sigma_c} \qquad (15)$$

Since the largest Mohr stress circle indicates a state of steady-state flow, the effective angle of internal friction φ_e *and* the measure of the internal friction, η at steady-state flow can be determined, $\eta = atan(\varphi_e)$. Differently from the Hausner ratio and Carr's index, which are based on an empirical method, the flow properties obtained from the measured yield loci are defined physical figures.

The most common method to determine the yield locus and the Morh's circle is to use a shear cell. To generate the yield locus the bulk solid specimen is repetitively loaded vertically by a normal stress (consolidation) and shear deformation is applied by a moving cell with a constant velocity which results in a horizontal shear stress (Jenike, 1961; Carr, & Walker, 1968; Shinohara, & Golman, 2002). Here the Schulze ring tester was employed and the methodology is extensively reported in the literature (Schulze, 2008).

2.5 Bulk powder compression

Confined compression of the powders was performed using a materials testing machine *Instron 5500* equipped with a cylindrical die with an internal diameter of 27.5 mm and flat-faced punches. The compression force was measured using a 15 kN load cell transducer. The movable top punch was made to descend in order to compress the powder samples until the maximum compaction force 12 kN was reached.

Table 2: Classification of the flowability function *ffc* (Fitzpatrick et *al.*, 2004).

Flowability	***ffc***
Not flowing	*<1*
Very cohesive	1-2
Cohesive	2-4
Easy-flowing	4-10
Free-flowing	>10

3 Results

3.1 Particle size and shape

SEM images, shown in Figure 5, were used to determine the sphericity for the spray dried zeolite particles.

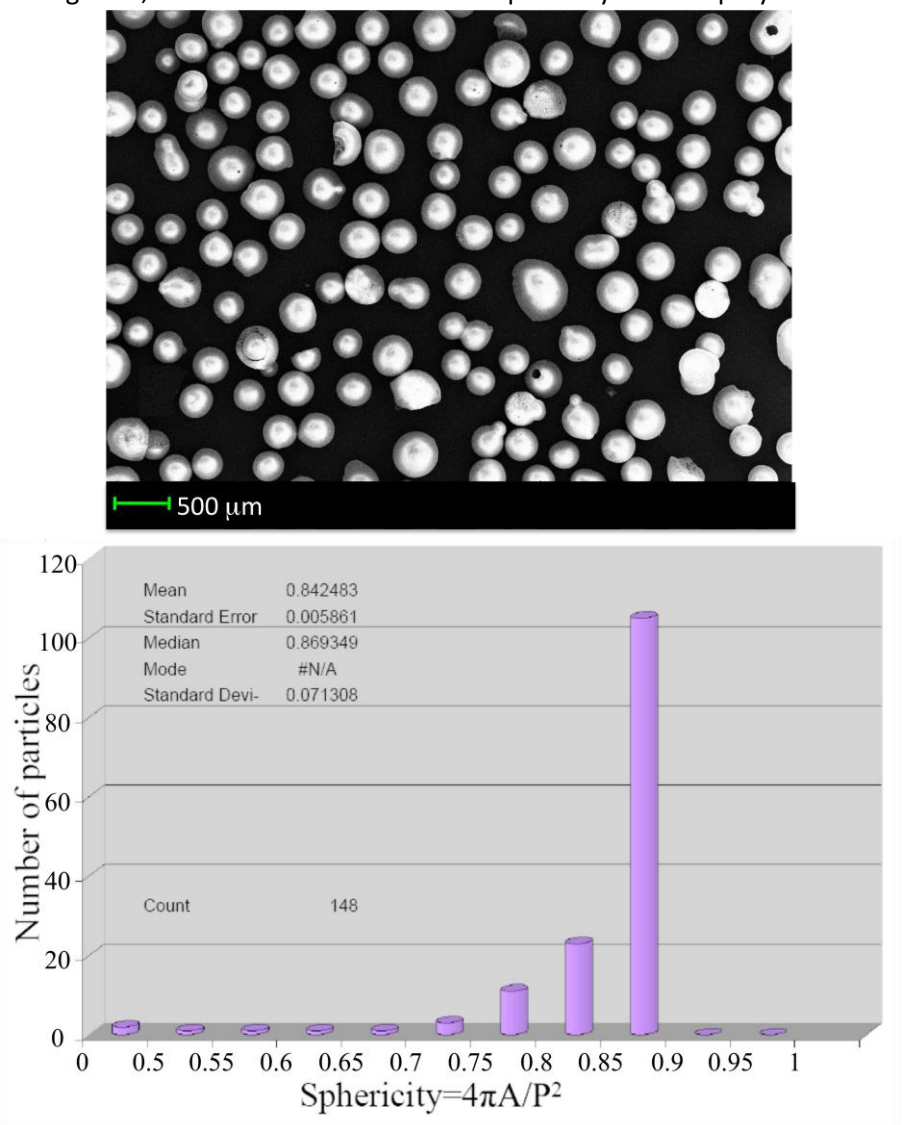

Figure 5: SEM images of spray dried ZSM5 zeolite and distribution of sphericity values.

The mean sphericity *S* of the sample of particle was calculated using Eq.(16) and the particle projected area.

$$S = 4\pi \frac{A}{P^2} \tag{16}$$

where *A* and *P* are the projected area and perimeter of the single particle, determined by image analysis. A perfect circle has sphericity of one while a very irregular object has sphericity closer to 0.

The particles considered in this work are spray-dried powders with a mean sphericity value of 0.84 and therefore they can be considered fairly spherical.

The particle size distribution is shown in Figure 6, with $d_{0.5}$=338 µm. The measurement using the Mastersizer 2000 was carried out in wet dispersion with a continuous ultrasonic level of 85%.

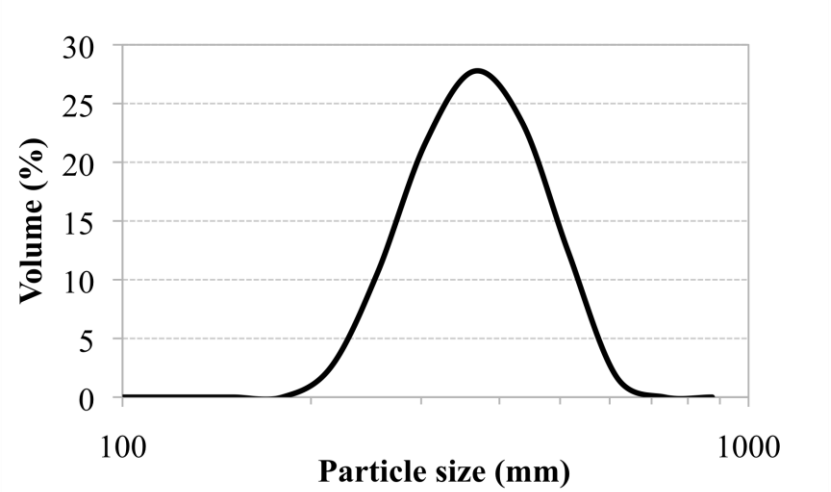

Figure 6: Particle size distribution for the zeolite sample.

3.2 Single particle characterisations

3.2.1 Micromanipulation: diametrical compression of single zeolite particles

To obtain statistically significant results at least 45 particles were randomly chosen and compressed at velocity of 0.01 mm s^{-1} until the rupture point. During the movement of the punch towards the upper fixed plate, contact between the particle and the fixed plate was created. During compression the punch displacement and compressive force were measured, as shown in Figure 7. The particle diameter can be inferred from the sudden increase of the measured force (tip touches the particle surface) and the breakage (failure) point corresponding to the sudden decrease in the load. The material appeared to be semi-brittle since the rate of drop in the force was dramatic.

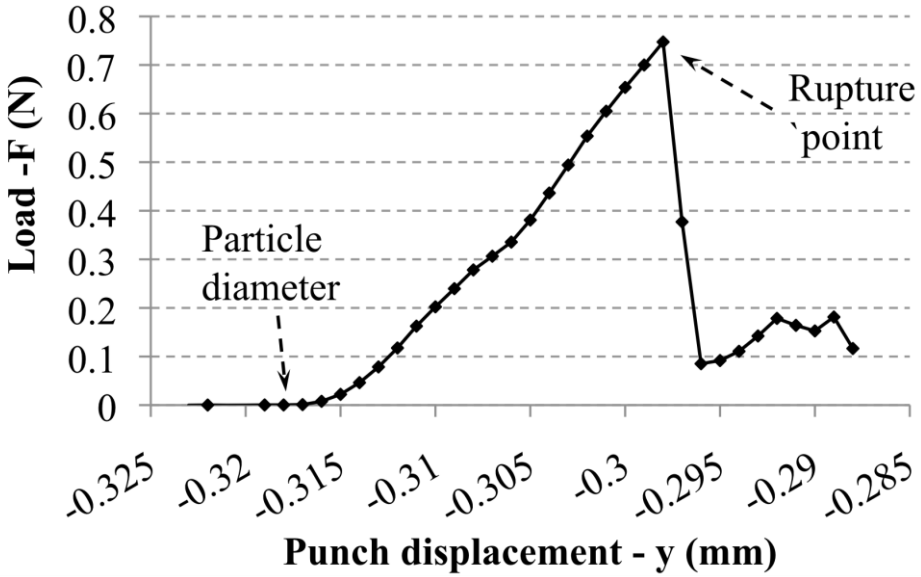

Figure 7: Typical force displacement curve for the zeolite particle using the Stable Microsystems analyser.

In Figure 8.a, the compression force against the local displacement is shown for a single particle. The reduced elastic modulus E^* was determined from the gradient of the linear fitting by plotting the load force F versus the local displacement $s^{3/2}$ according to Eq.(7), Figure 8.b.

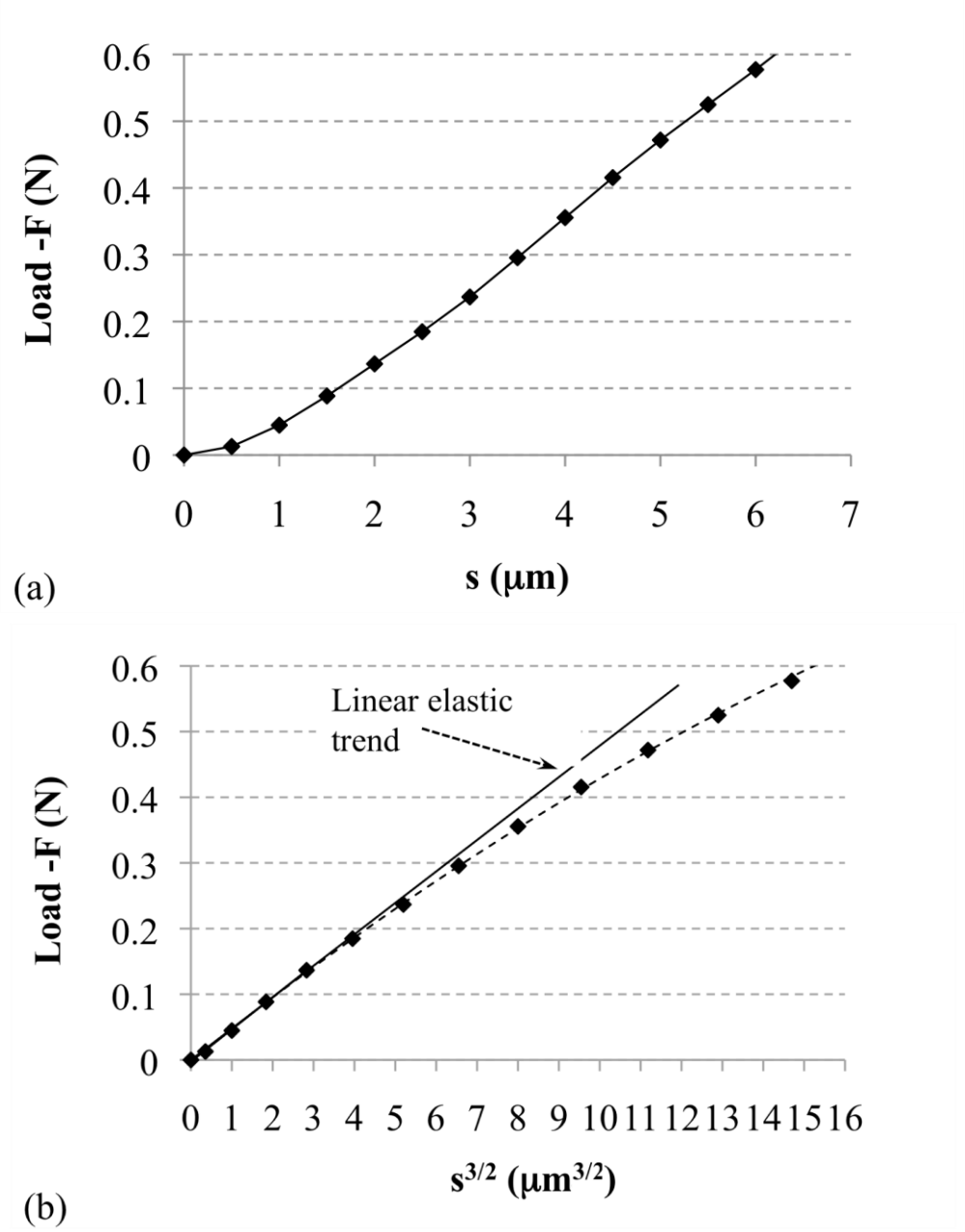

Figure 8: Data for single particle compression (a) local displacement (b) data plotted according the Hertz contact theory and linear fitting.

The elastic modulus, defined in Eq.(8), is commonly employed in micromanipulation studies and assumes an isotropic material behaviour. Spray dried zeolite particles, however, are microporous inorganic composites which contain small pores and therefore they can exhibit anisotropic behaviour. Therefore, the elastic modulus value determined here should be considered as an effective specific particle value, rather than the absolute material property of the zeolite particles. The variation of the reduced elastic modulus with particle size is shown in Figure 9.a and the average value for E^* was equal to 2.93±0.63 GPa.

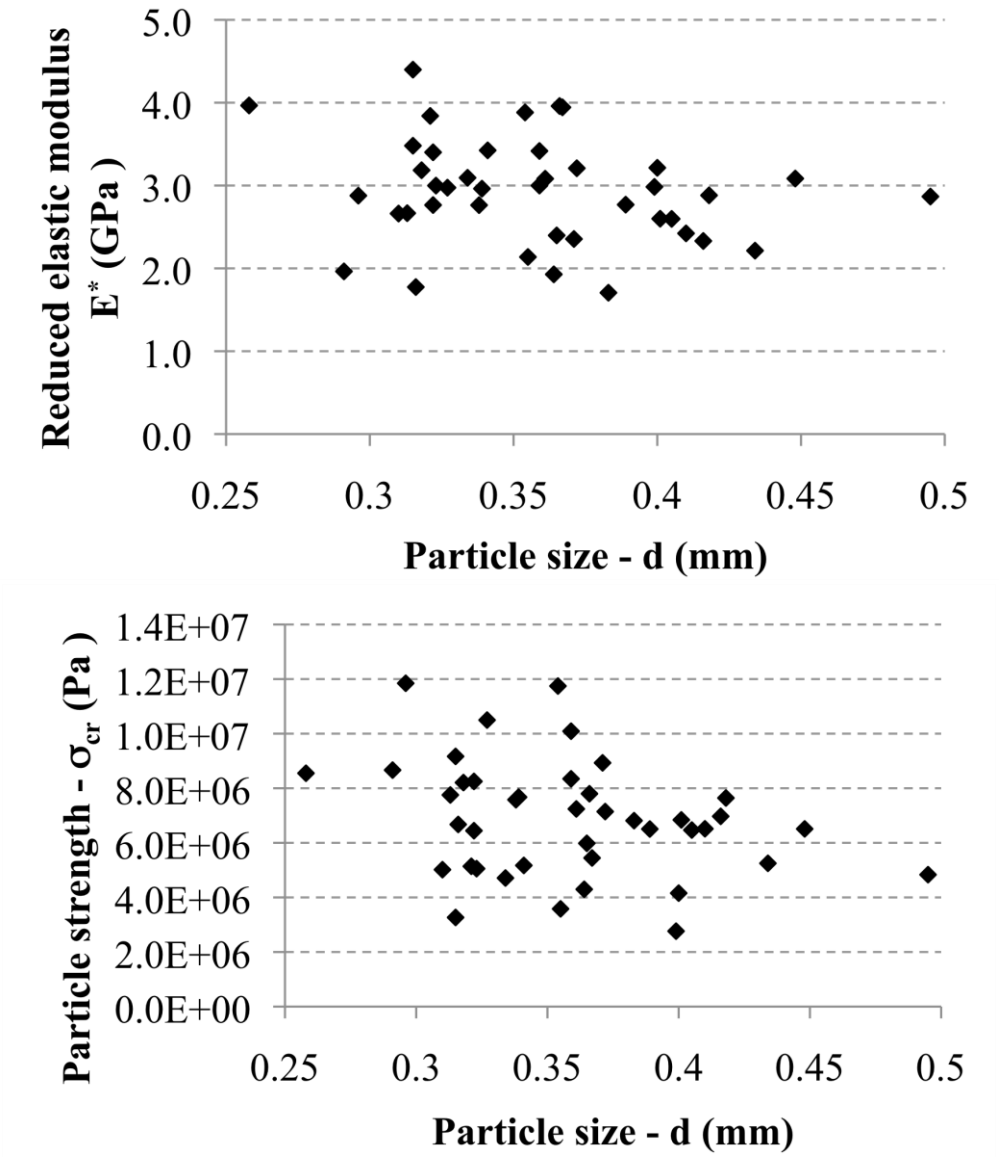

Figure 9: (a) Reduced elastic modulus. (b) Nominal rupture stress of single zeolite particle.

The peak compression force, called the breakage point, was used to calculate the nominal rupture stress, Eq.(9), and the mean nominal rupture stress was 981±321 mN, Figure 9.b. The value for the standard deviation is high, showing large variation on mechanical properties within the sample. This type of material can have a wide strength distribution due to the presence of defects, pores and binders, causing early breakage of the weakest particles. Moreover, the distribution of flaws size, shape, and orientation can differ from sample to sample.

The data from the compression test can be fitted to a statistical model to quantify the spread of the sample of particles. The Weibull statistical strength distribution has been shown to be an appropriate model to describe failure of brittle materials (Weibull, 1951). This is a two parameters distribution function and the relationship between the cumulative probability of failure, P_f, at or below a stress, σ, is calculated as follows:

$$P_f = F(\sigma_{cr}) = 1 - e^{-\left[\left(\frac{\sigma_{cr}}{\sigma_0}\right)^m\right]} \quad (17)$$

Where σ_{cr} is the failure stress (particle strength) and m is the characteristic strength distribution parameter (Weibull modulus). σ_o corresponds to the crushing stress with a fracture probability of 63.2%. The parameter m represents the nature, spread and dispersion of flaws and defects. In particular, a low value for m indicates a non-uniform broad distribution of flaws that leads to a broad distribution in strength. A high value for m indicates

a narrow and uniform distribution of defects and, therefore, smaller strength distribution.
The two parameter modulus *m* and σ_o from the Weibull can be extrapolated by linear regression of the strength data; thus Eq.(17) can be written as follows:

$$\ln\left[\ln\left(\frac{1}{1-P}\right)\right] = m\ln\sigma_{cr} - m\ln\sigma_0 \qquad (18)$$

For a set of experimental measured fracture stresses, it is necessary to assign a probability of failure by ranking the experimental strength data σ_{cr} and assigning a probability of failure P_i to each stress σ_i ($\sigma_i = \sigma_{cr}$ for the particle i). Since the true value of P_i is unknown, a prescribed estimator has also to be defined, in this work the estimator described by Eq.(19) has been employed (Sullivan, & Lauzon, 1986).

$$P_i \approx \frac{i-0.3}{n+0.4} \qquad (19)$$

where P_i is the probability of failure for the *i* ranked strength data, and *n* is n is the total number of particle crushing test observations.
The parameters *m* and σ_o (*m*=3.2 and σ_o=10.8 MPa) are determined from the slope and intercept of the trend line as shown in Figure 10, plot of $ln[ln(1/(1-P_i))]$ versus $ln\sigma_{cr}$.

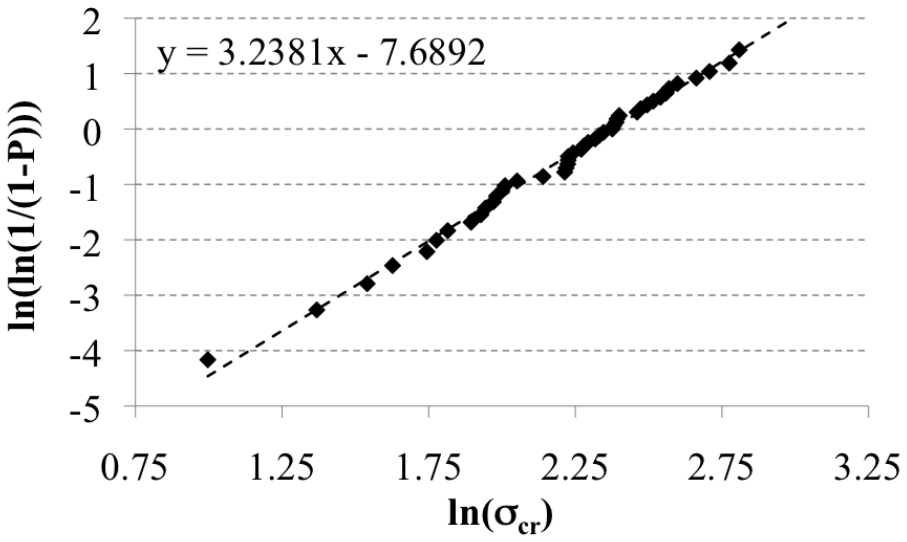

Figure 10: Cumulative distribution function for the zeolite sample, determination of the Weibull modulus *m* (dashed line).

3.2.2 Nanoindentation: of zeolite particles

The ZSM5 zeolite particles were held on the sample holder by adhesive glue (Loctite® 496™, methyl cyanoacrylate, Henkel, UK). The diamond tip was pressed against the particle surface to create the indent and the load and displacement were monitored continuously. Four levels of indentation depth, 1, 4, 5 and 6 µm, were considered. The Young's modulus and hardness were determined using Eq.(10) and Eq.(12).
Each indentation experiment consisted of six segments as shown in Figure 11. Initially, the tip approaches the surface of the particle. Once the indenter touches the surface the loading is applied until the desired indentation depth (A). The load is held constant (B) for the desired time (30 seconds for 1 µm and 20 seconds for 4,5,6 µm) to assess possible creep or mechanical stabilization (relaxation). In segment (C) 90% of the maximum load was removed then held for 30 seconds, segment (D). This hold segment, inserted after a partial unloading segment, can be used to correct for the thermal drift of the apparatus during the indentation process (Wimmer, Lucas, Tsui, & Oliver, 1997). During segment (E) the indent is totally unloaded from the particle surface.

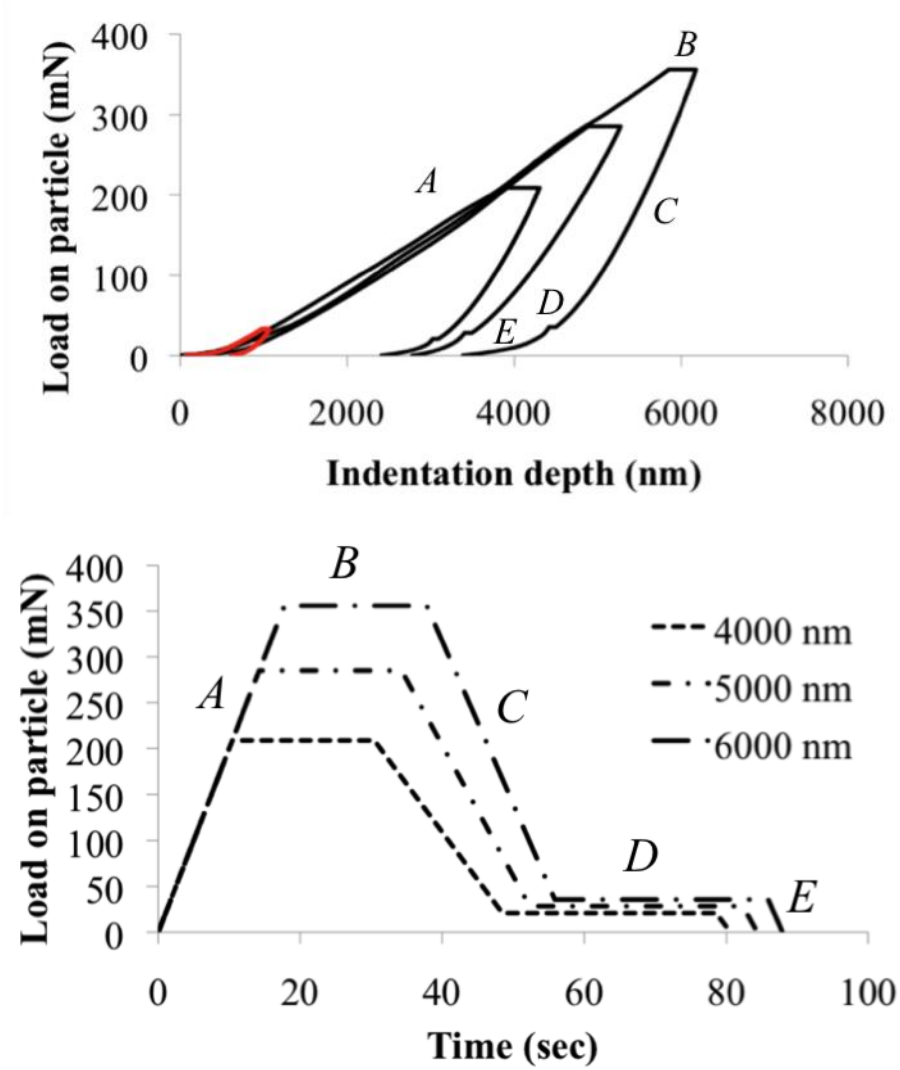

Figure 11: (a) Typical load and unload curves for a zeolite particles with different levels of indentation depth: 1, 4, 5 and 6 µm.

In Figure 12, the Young's modulus and hardness are shown over the indentation depth for 13 different indentation experiments on zeolite particles. It can be seen that there is a decrease in Young's modulus and hardness with indentation depth. This is called indentation size effect, wherein the hardness is observed to increase with decreasing indentation size. This is due to a lower number of dislocations necessary to create a permanent shape change with increasing indentation depth, which results in decreasing hardness and Young's modulus values (Gan, & Gu, 2008).

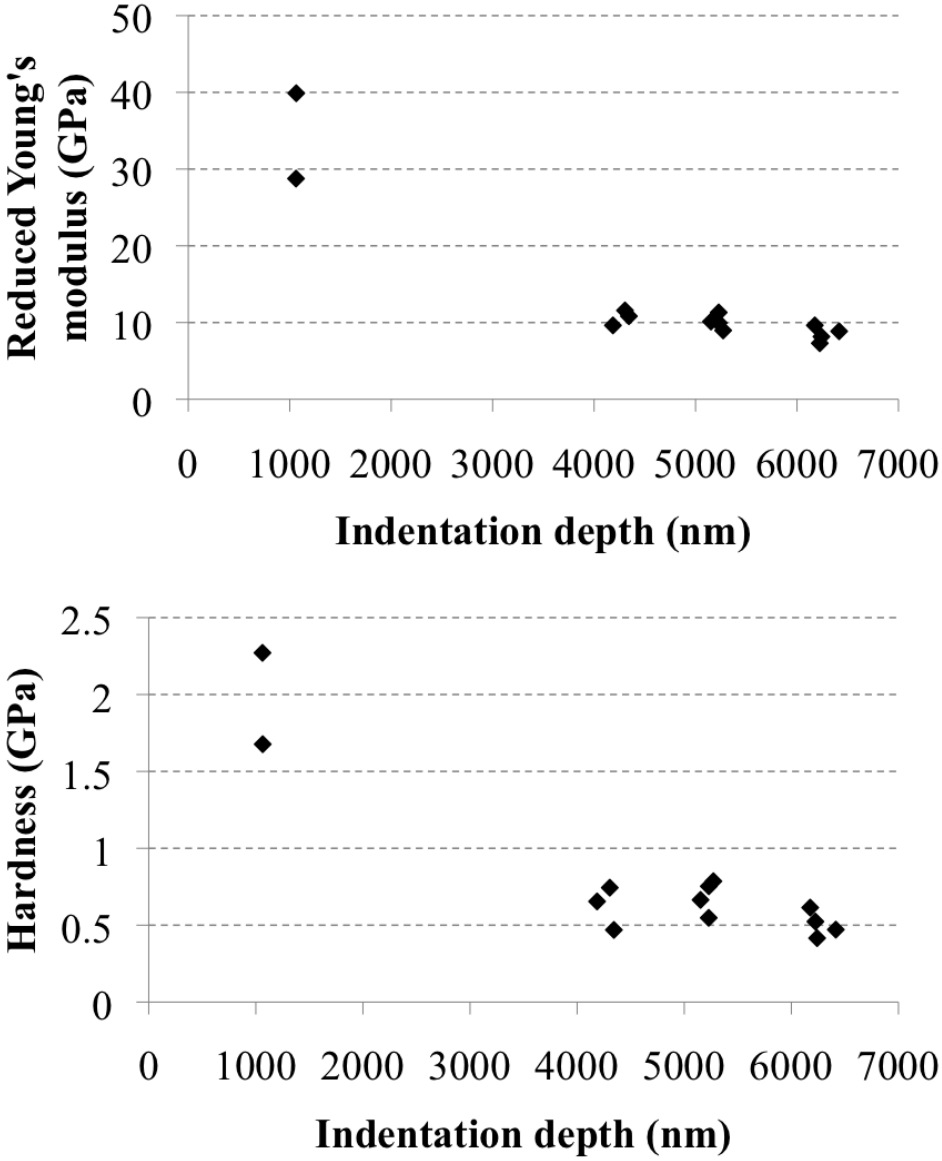

Figure 12: (a) Reduced Young's modulus. (b) Hardness during indentation.

The indentation size effect decreased with increased indentation depth. At higher indentation depths the Young's modulus and the hardness were less variable. The elastic modulus and hardness had an indentation size effect. The average values of reduced Young's modulus E^* and hardness H for each indentation depth are given in Table 3.

Table 3: Average values for the reduced Young's modulus E^* and hardness H for each indentation depth with standard deviations.

Indentation depth considered (nm)	**H (GPa)**	**E^* (GPa)**
1000	1.97±0.42	34.32±7.86
4000	0.62±0.14	10.67±0.98
5000	0.68±0.10	10.09±0.96
6000	0.51±0.08	8.49±0.99

3.3 ZSM5 powder flowability: Hausner ratio, Carr's index and flow function (ffc)

The results for the Hausner ratio and Carr's compressibility index, Table 4, showed the excellent flowability. The bulk poured and tapped densities reported are much lower than the skeletal density of the material measured by helium pycnometry as the latter excludes the micro and nano porosities of the particles and the voidage between the packed particles. The excellent flow property of the zeolite particles was probably the result of the spherical morphology and narrow range of particle size distribution. To confirm the excellent flowability of this material the Schulze ring test was also conducted.

Table 4: Measured zeolite flow properties: Hausner ratio, Carr's index and flow function.

Characteristic	**Zeolite**
Bulk poured density (g/cm^3)	0.672
Tapped density (g/cm^3)	0.693
Hausner ratio – HR	1.03z (excellent flow)
Carr's Index – CI	3.301 (excellent flow)
Average bulk density (Schulze ring test)	0.722
$ffc_{average}$ (Schulze ring test)	69.5 (excellent flow)

The flowability of the ZSM5 zeolite sample was characterised by using a Schulze ring tester which provided bulk quantitative experimental values at consolidated states for the flowability function *ffc*, the particle-particle angle of internal friction φ_e and the bulk density. The shear cell was filled with the powder sample and the excess of powder was scraped off with a spatula. The sample was carefully weighted to determine the bulk density. The sample was loaded under three levels of normal load and then sheared, Figure 13. The result regarding the flow function *ffc* for the zeolite sample is reported showing the excellent flowability for the material with an average

value of $ffc_{average}$ equals to 69.5. The average values for the angle of friction, φ_e, and internal coefficient of friction, η, were respectively 27.8° and 0.452.

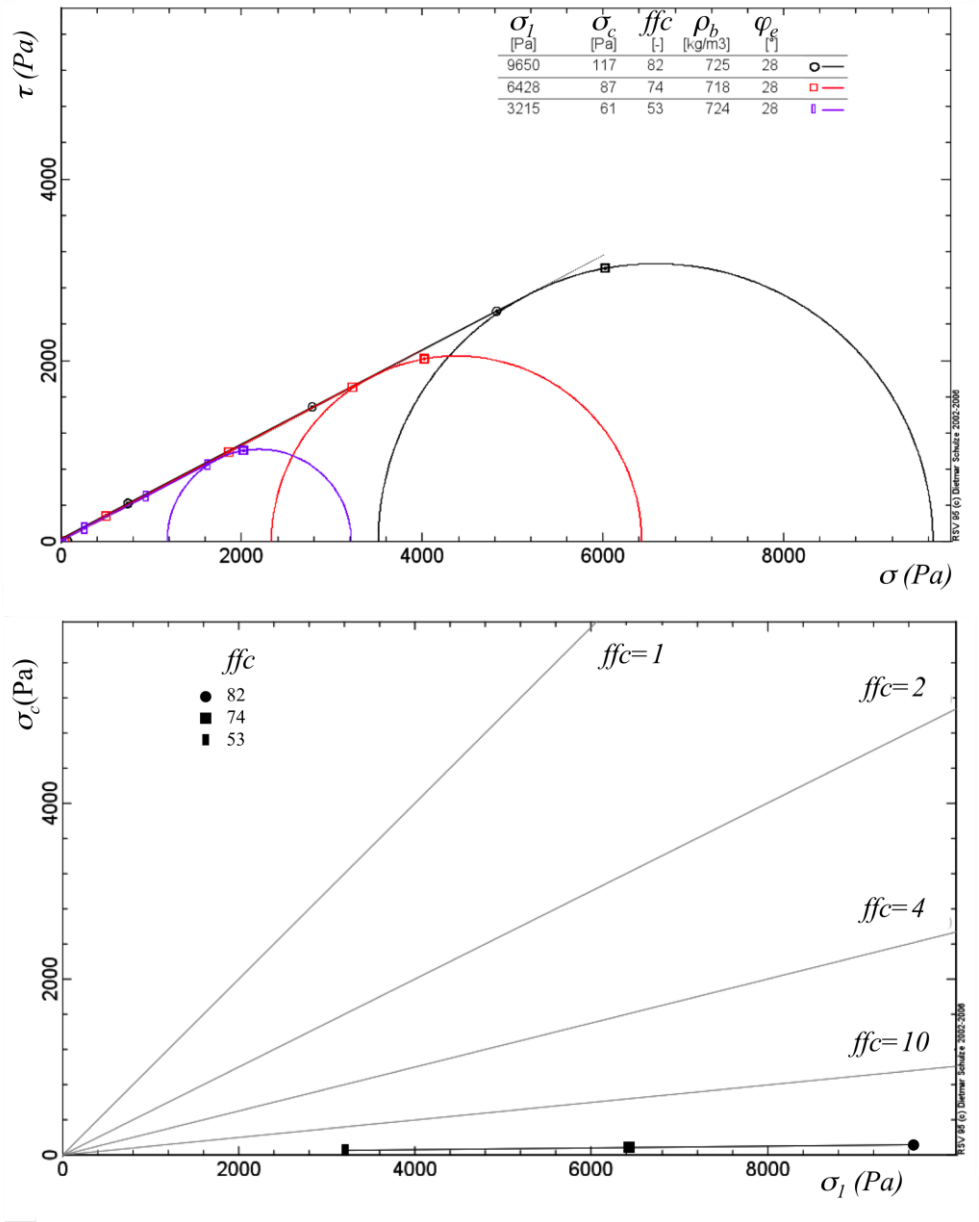

Figure 13: (a) Zeolite yield locus for the normal load at pre-shear equals to 2000 (purple), 4000 (red), 6000 (black) Pa. (b) Zeolite unconfined yield strength σ_c versus consolidation stress σ_1 and flow function *ffc*.

It is interesting to note in Table 4 that all the three measurements for the poured bulk density poured, tapped density and average bulk density from the Schulze ring tester were very similar. This shows the poor compressibility of the powder bed, which is also demonstrated later by using bulk powder compression.

3.4 Bulk powder compaction for the zeolite ZSM5 sample

The amount of powder introduced into the die for each test was pre-weighed. The displacement-force data were collected and transferred to a computer. The initial powder bed height was recorded when contact was first made between the punch surface and the bed. The aspect ratio was calculated from the recorded bed height. Tablets were compressed at different punch speeds (from 0.01 up to 0.8 mm s^{-1}). The stress transmission and stress distribution during the compression process could be affected by the aspect ratio A.R., ratio of the initial bed height to powder bed diameter. Therefore, in order to evaluate the potential influence of this ratio on the

derived bulk compression parameters, different bed aspect ratios were considered, by pouring different quantity of material into the die.

In Figure 14.a typical compression pressure strain curves are reported for bulk compression of zeolite particles at different punch speeds. It can be observed that there is no major variation in the trends for the compaction behaviour with punch speed. Considering the bulk compression curve for one of the tablet (T1), Figure 14.b, three different changes in slope can be observed. These represent the different densification behaviour of the powder bed during the compression. During the *first stage*: the powder densification is low (steeper slope) probably due to that the particles are very hard and probably only deform elastically, bulk bed density slightly increases due to particle rearrangement. During the *second stage* the bulk of bed is probably deforming plastically, particle breakage is occurring with a decrease in bed voidage (higher bed densification). During the *third stage* the voidage has reduced and bulk and the bed densification decreases. During this stage the entire bulk of material is probably deforming elasto-plastically.

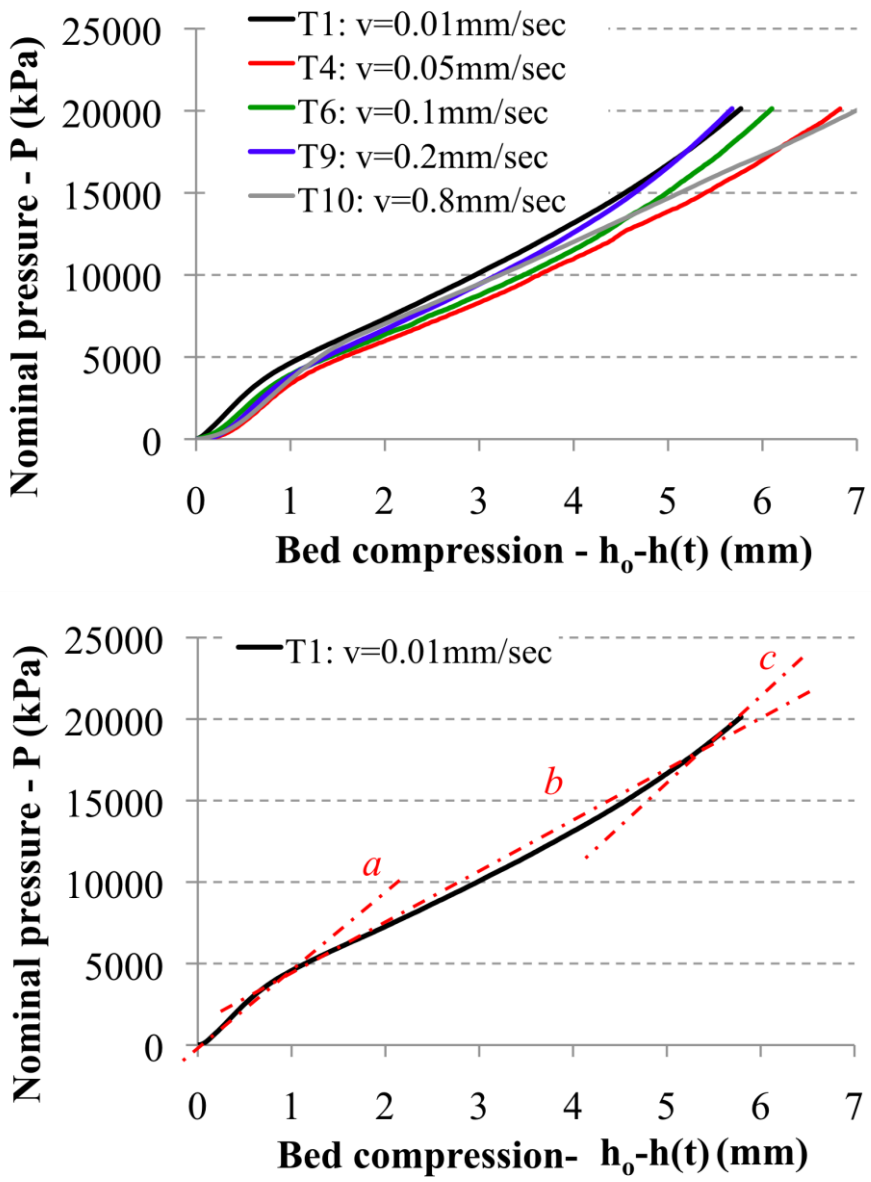

Figure 14: (a) Nominal pressure *P* against punch displacement curves for the bulk compression for different punch speed. (b) Bulk compression for zeolite particles for different punch speed.

3.4.1 Adams plots for zeolite ZSM5

The data were used to fit the Adams model and in Figure 15 the Adams plot over full the compression load (12 kN) is showed for the tablet T1.

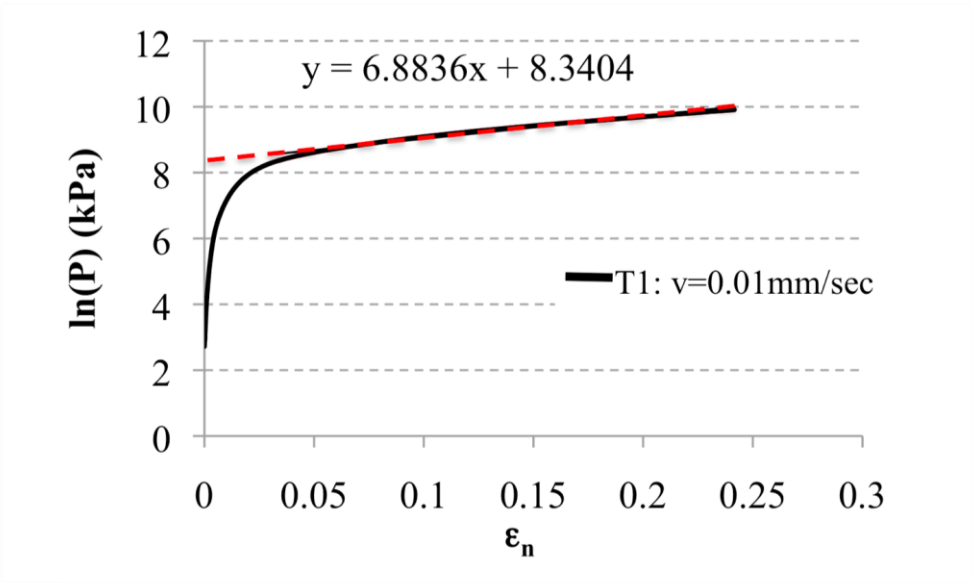

Figure 15: Adams compression curve for tablet T1 and linear fitting compression curves for table T1 up to 12000 N normal load, Adams relationship.

The parameters $\tau_o^{'}$ and $\alpha^{'}$ were thus determined over the full compression range by linear regression in the linear interval as depicted in Figure 15 according to the Adams relationship, Eq.(4). Figure 16 shows the parameters (apparent strength of the single particles $\tau_o^{'}$ and the apparent coefficients of friction $\alpha^{'}$) from the Adams model as a function of the initial aspect ratio (A.R). The aspect ratio had an effect on the bed compressibility, probably as a function of wall friction (Samimi et *al.*, 2005). Therefore, the apparent strength of the single particles $\tau_o^{'}$ and the apparent coefficient of friction $\alpha^{'}$ have been extrapolated by linear fitting at zero aspect ratio A.R. and reported in Table 5, where a comparison between the Adams model parameters obtained by bulk compression and the results from the single particle compression are shown.

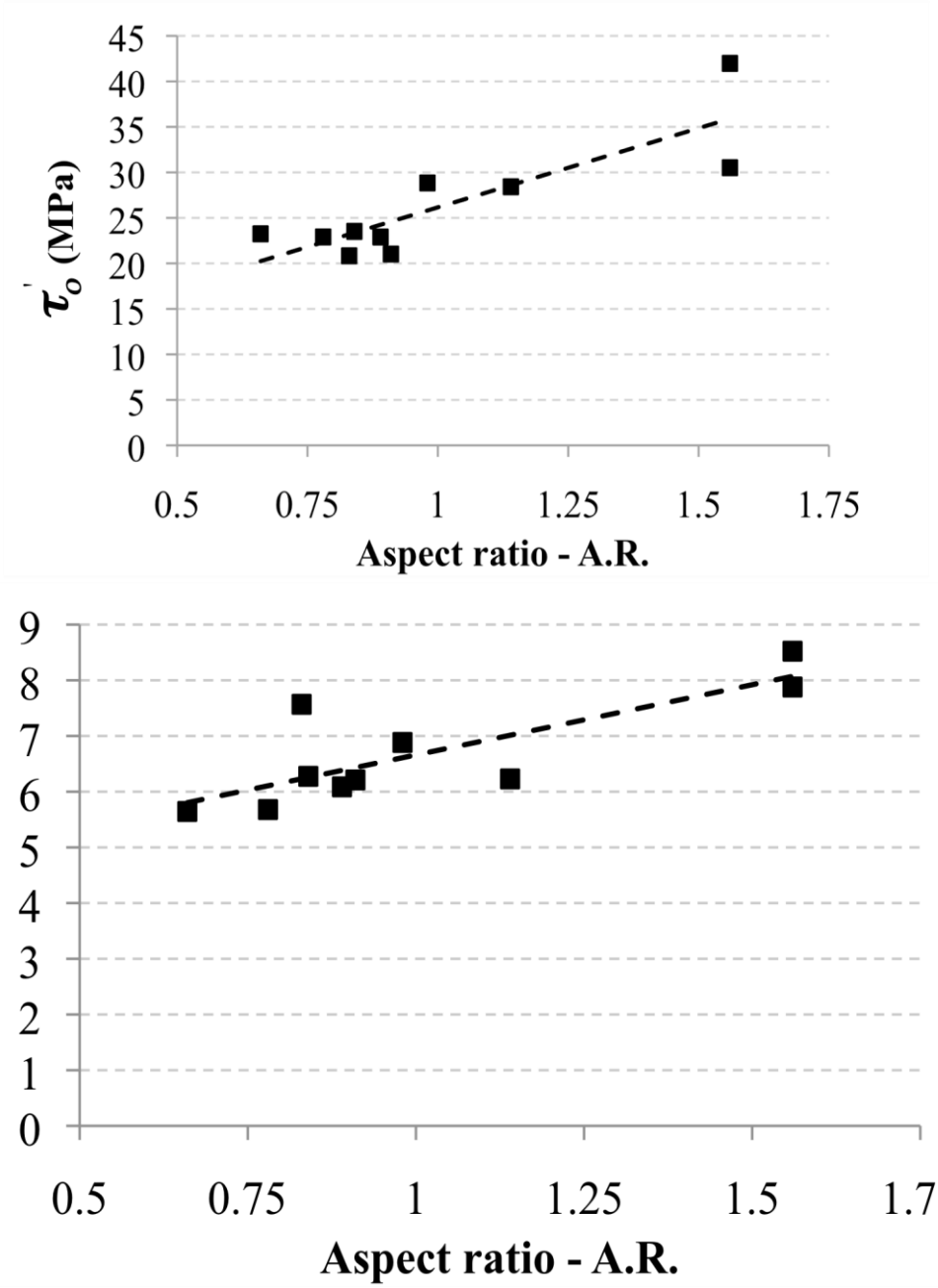

Figure 16: Effect of aspect ratio A.R. on τ_o' and α' parameters from the Adams model.

Table 5: Average values of bulk compression parameters from the Adams model compared with single particle compression tests and by Nanoindentation. Only the apparent strength from the Adams model is comparable with single particle strength data.

Adams (A.R.=0)		**Single particle compression**		**Nanoindentation**
α'	τ_o' (MPa)	σ_{cr} (MPa)	σ_0 (MPa)	**H** (GPa)
4.14	8.76	9.8	10.8	0.604 - 1.973

From the previous table it can be observed that the Adams model, which was developed for granules, seems to fit the bulk compression data according as the predicted apparent strength of the single particles τ_o'. This

parameter was in good agreement with the particle strengths σ_{cr} and σ_o determined by single particle compression testing (σ_{cr} particle crushing strength and σ_o crushing strength with a fracture probability of 63.2%).

4 Conclusions

The mechanical properties for ZSM5 zeolite particles have been characterized by using different powder characterisation techniques. Mechanical properties such as reduced elastic Young's modulus, yield stress and particle strength was characterised by single particle compression test. Hardness and reduced elastic Young's modulus were also measured by Berkovich nanoindentation and they were found to be proportional to the indentation depth. The elastic modulus measured by nanoindentation (between 9.6 and 34.3 GPa) was found to be significantly different from the value obtained by single particle compression (2.93 GPa). Differences in the values between the two techniques probably indicate the heterogeneity of the porous particles in terms of mechanical properties. The excellent flowability of the material was described using methods such as Carr's index and Hausner ratio. The internal particle-particle friction coefficients and flow function were measured as bulk measurement at different consolidated states by using a Schulze shear cell. Again, it was observed that zeolite spray dried particles had exceptional flowability and the poor particle compressibility would not be related to friction effects during particle rearrangements. The poor compressibility was also demonstrated by bulk powder compression tests. These showed that at low pressure the densification was low, which was probably due to the high particle strength and particle hardness. It was also found that the Adams model seems to describe the experimental bulk compression data and the predicted Adams parameter, apparent strength for the single particles $\tau_o^{'}$ was in good agreement with the particle strength determined by single particle compression test, σ_{cr}.

In this work, it was shown how a comprehensive description of mechanical properties for a powder material, in this case zeolite particles, is essential in order to understand its bulk behaviour in a process such as bulk compaction. A complete assessment of particulate material characteristics is necessary in order to the design better process involving such form of materials.

Acknowledgement: MM would like to acknowledge the EU for financial support through the Framework 6 Marie Curie Action "NEWGROWTH", contract number MEST-CT-2005-020724, Johnson Matthey Plc for funding and supporting this research.

5 References

Adams, M.J., Mullier, M.A., & Seville J.P.K. (1994). Agglomerate strength measurement using a uniaxial confined compression test, *Powder Technology*, 78, 5–13.

Caligaris, R.E., Topolevsky, R., Maggi, P., & Brog F. (1985). Compaction behaviour of ceramic powders, *Powder Technology*, 42, 263-267.

Carr, J.F., & Walker, D.M. (1968). An annular shear cell for granular materials, *Powder Technology*, 1, 369-373.

Djuri, M., Marinkovi-Neduin, R., Ranogajec, J., & Radeka, M. (1995). Particle size range as a factor influencing compressibility of ceramic powder, *Ceramics International*, 21, 227-230.

Fitzpatrick, J.J., Barringer, S.A., & Iqbal, T. (2004). Flow property measurement of food powders and sensitivity of Jenike's hopper design methodology to the measured values, *Journal of Food Engineering* 61, 399-405.

Frenning, G., Nordström, J., & Alderborn, G. (2009). Effective Kawakita parameters for binary mixtures, *Powder Technology,* 189, 270-275.

Gan, K. & Gu, M. (2008). The compressibility of Cu/SiC_p powder prepared by high-energy ball milling, *Journal of Materials Processing Technology,* 199, 173-177.

Greyand, R.O., & Beddow, J.K. (1969). On the Hausner, Ratio and its relationship to some properties of metal powders, *Powder Technology*, 2, 323-326.

Hausner, H.H. (1967). Friction conditions in a mass of metal powder, International Journal of Powder Metallurgy, 3, 7-13.

Hertz H. (1882). Über die Berührung fester elastischer Körper, *Journal fur die Reine und Angewandte Mathematik*, 92, 156–171.

Jenike, A.W. (1964). Storage and flow of solids, *Utah Eng Exp Stn Bull.,* 123, 1-194.

Jenike A.W. Gravity flow of bulk solids (1961). *Utah Eng Exp Stn Bull.*, 108, 1-294.

Klevan, I., Nordström, J., Bauer-Brandl, A., & Alderborn, G. (2009). On the physical interpretation of the initial bending of a Shapiro–Konopicky–Heckel compression profile, *European Journal of Pharmaceutics and Biopharmaceutics*, 71, 395-401.

Klevan, I., Nordström, J., Tho, I., & Alderborn, G. (2010). A statistical approach to evaluate the potential use of compression parameters for classification of pharmaceutical powder materials, *European Journal of Pharmaceutics and Biopharmaceutics,* 75, 425-435.

Lin, J., Shu, X.F., & Dong, J.X. (2005). The experimental determination of mechanical properties of zeolite ferrierite crystal, *Materials Letters*, 59, 1595-1597.

Meier, M., John, E., Wieckhusen, D., Wirth, W., & Peukert, W. (2009). Influence of mechanical properties on impact fracture: Prediction of the milling behaviour of pharmaceutical powders by Nanoindentation, *Powder Technology,* 188, 301-313.

Michrafy, A., Ringenbacher, D., & Tchoreloff, P. (2002). Modelling the compaction behaviour of powders: application to pharmaceutical powders, *Powder Technology,* 127, 257-266.

Ramakrishnan, K.N., Nagarajan, R., RamaRao G.V., & Venkadesan, S. (1997). A compaction study on ceramic powders, *Materials Letters*, 33, 191-194.

Samimi, A., Hassanpour, A., & Ghadiri, M. (2005). Single and bulk compressions of soft granules: Experimental study and DEM evaluation, *Chemical Engineering Science*, 60, 3993-4004.

Schulze D. (2006). Flow properties of Powders and Bulk Solids [online]. Available: http://www.dietmar-schulze.de/grdle1.pdf, [accessed June 2010].

Schulze, D. (2008). A test with the Ring Shear Tester RST-XS [online]. Available: http://www.dietmar-schulze.de/leaflxse.pdf, [accessed June 2008].

Shinohara, K., & Golman, B. (2002). Dynamic shear properties of particle mixture by rotational shear test, *Powder Technology*, 122, 255-258.

Sivasankaran, S., Sivaprasad, K., Narayanasamy, & R., Iyer, V.K. (2010). An investigation on flowability and compressibility of AA 6061100 – *x*-*x* wt.% TiO2 micro and nanocomposite powder prepared by blending and mechanical, alloying, *Powder Technology,* 201, 70-82.

Stable Micro System LTD, (2010). Catalysts seeking the next big thing, Chemical Week [online]. Available: http://www.stablemicrosystems.com, [accessed December 2010].

Stasiak, M., Tomas, J., Molenda, M., Rusinek, R., & Mueller, P. (2010). Uniaxial compaction behaviour and elasticity of cohesive powders, *Powder Technology*, 203, 482-488.

Sullivan, J.D., & Lauzon, P.H. (1986). Experimental probability estimators for Weibull plots, *Journal of Materials Science Letters*, 5,1245–1247.

Vogler, T.J., Lee, M.Y., & Grady, D.E. (2007). Static and dynamic compaction of ceramic powders, *International Journal of Solids and Structures*, 44, 636-658.

Weibull W. (1951). A statistical distribution function of wide applicability, *Journal of Applied Mechanics*, 18, 293–297.

Wimmer, R., Lucas, B.N., Tsui, T.Y., & Oliver, W.C. (1997). Longitudinal hardness and Young's modulus of spruce tracheid secondary walls using nanoindentation technique, *Wood Science and Technology* , 31, 131–141.

Yap, S.F., Adams, M.J., Seville, J.P.K., & Zhang, Z. (2008). Single and bulk compression of pharmaceutical excipients: Evaluation of mechanical properties, *Powder Technology,* 185, 1-10.

Zhang, Z., Seville, J.P.K. , Adams, M., & Yap, S.F. (2006). Understanding the mechanical properties of single micro-particles and their compaction behaviour, *China Particuology*, 4, 35-40.